Hindawi
Shock and Vibration
Volume 2023, Article ID 6668089, 11 pages
https://doi.org/10.1155/2023/6668089

Research Article

Study on the Influence of the Internal Elastic Constraint Stiffness on the Vib-Acoustic Performance of a Coupled Plate-Cylindrical Shell System

Yonggan Sun [1,2] **and Yong Xiao** [1]

[1]*School of Civil Engineering, Chongqing Jiaotong University, Chongqing 400074, China*
[2]*Chongqing Steel Structure Industry Limited Company, Chongqing 400037, China*

Correspondence should be addressed to Yonggan Sun; sunygqj@163.com

Received 1 February 2023; Revised 6 May 2023; Accepted 29 June 2023; Published 24 July 2023

Academic Editor: Xiang Liu

Regarding the vib-acoustic performance of internal coupled structures, basically all relevant studies have been confined to the classic form of connections. In this investigation, the boundary and internal elastic constraint matrices of the coupled structure are established, the vibration and sound calculation model of the coupled structure is then established, and numerical analysis is performed to show the effect of constraint stiffness on the vibration and acoustical performance of a coupled plate-cylindrical shell system. The results show that impedance matching between the structures is improved with the increase of the elastic connection stiffness, which is conducive to the vibration energy propagation. Moreover, the supporting coupling stiffness between elastic coupled structures plays an important role in vibration energy transfers.

1. Introduction

The dynamic behavior of different structures and a series of problems caused by them have been the focus of research [1–5]. It is well known that cylindrical shells separated by longitudinal bottom plates are important simplified structures in ocean engineering, aerospace engineering, and other fields. Therefore, it is necessary to further investigate the vibration and acoustic properties of the plate-cylindrical shell coupling system.

Although there are many studies on the coupled plate-cylindrical shell systems, the internal connections of these structures are usually assumed to be rigid and fixed. Missaoui and Cheng combined the artificial spring technique with the integral mode method to build a numerical model to discuss the sound performance of the shell system [6]. To better understand the internal physical mechanisms and offer advice on noise and vibration management, Li et al. studied the acoustic propagation property interaction between a cylindrical shell with compartments and a constrained acoustic enclosure [7]. Wang et al. studied the power flow characteristics of a complicated plate-cylindrical shell system by using the receptance substructure approach, and the theoretical description of the mode shape function was employed to represent the receiving function of each substructure [8]. Zhao et al. established the receptivity expression of plates and shells by using the conventional plate theory and Loew's shell theory. Based on the geometric compatibility constraints and force balancing, they were able to develop the frequency equation for shell and plate-coupled systems and analyze the vibration transmission properties of cylindrical shells [9]. The researchers Clot et al. developed a cogent model for a double-deck tunnel. The model considered the pipe model to describe the coupling system. The computational findings indicate that there is a discernible distinction between the two types of tunnels, with the double-layer tunnel exhibiting a greater capacity for the passage of radiant power [10]. By applying the reciprocity theorem, Zou et al. was able to determine the characteristic of underwater acoustic radiation that is

produced by an infinitely long structure consisting of an inner plate and a cylindrical shell [11]. Deng et al. conducted their research on a composite cylinder shell that had an interior thin plate and a number of acoustic black holes inserted within the plate. They solved the structural modal parameters by employing the Gaussian expansion approach, and they decreased the order of the model by utilizing the modal truncation technique [12]. In order to study the dynamic characteristics of cylindrical shells that have an internal flexural floor structure, Tian et al. developed a formula that combined analytical and numerical methods. The entirety of the construction may be broken down into three distinct parts: the cylinder shell, the axisymmetric ring plate, and the nonaxisymmetric floor plate [13]. Taking into account the displacement continuity requirement, Zhao et al. derived the coupling controlling equation of a spinning constructed cylinder of shell plates by using the Donnell shell theory, the Kirchhoff plate theory, and the Lagrange equation. Free vibration results for the combined cylinder shell and plate structure are calculated by using the assumption mode approach [14]. For a simply supported shell system, Lee et al. were able to determine the system's natural frequency as well as its mode function by employing the Rayleigh–Ritz method, which is predicated on the principle of energy. In addition, they were able to determine the dynamics behavior of a cylindrical shell with an inner plate by employing the tolerance method [15].

According to an analysis of the relevant published research, earliest investigations on plate-cylindrical shell coupling architectures were restricted to clamped or hinging systems.

Regarding the vib-acoustic performance of the coupled structure, basically all the studies have been confined to the classic form of connections, such as welding or hinging. However, there are numerous different instances of elastically connected structures in the actual application of engineering, for instance, space vehicles, building structures, and ship hulls, as shown in Figure 1. According to the knowledge of the author, few works have been reported on the vibrational and acoustic performance of elastically linked structures. In addition, the particulars of the vibrational and acoustic behavior, as well as the processes that underlie this behavior in such elastically linked materials, are not yet completely known. The primary objective of the research is to contribute in bridging this research gap. In the future, when a better knowledge of the interactions between elastically coupled plate-cylindrical shell systems is achieved, it will be possible to gain insight into how elastically coupled structures may be utilized in the control of vibration and noise in real settings.

There are four sections in this paper. The first part of the paper is the introduction. The corresponding matrix representation is provided in Section 2. In Section 3, the impacts of the internal constraint stiffness on the vib-acoustic performance of structures are discussed. The main results of this paper are summarized in the final section.

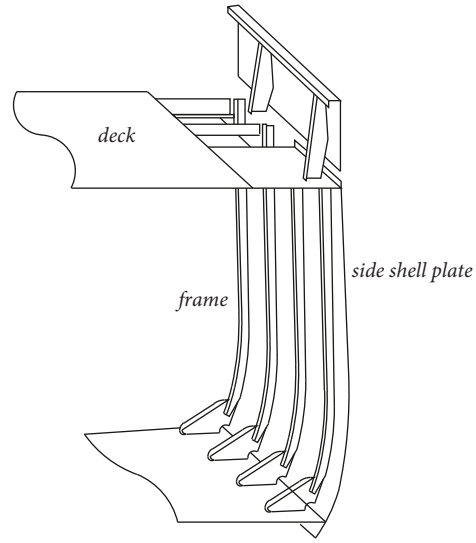

Figure 1: The connection form of the ship hull structure.

2. Theory

2.1. Modelling of the Shell Element. A point (x, y, z) within the element is made to have a displacement that takes the following form [16]:

$$\begin{cases} U(x, y, z) = u(x, y) + z\theta_x, \\ V(x, y, z) = v(x, y) + z\theta_y, \\ W(x, y, z) = w(x, y). \end{cases} \tag{1}$$

In the above formula, the displacement of the corresponding points is represented by u, v, and w; meanwhile, the midplane's rotations are represented by θ_x and θ_y, respectively.

According to the Mindlin bending theory, the shell's strain components are as follows [17]:

$$\begin{aligned} \left\{\varepsilon_0^P\right\} = \{&u_{,x}\, v_{,y}\, u_{,y} + v_{,x}\, \theta_{x,x}\, \theta_{y,y}\, \theta_{x,y} \\ &+ \theta_{y,x}\, w_{,y} + \theta_y\, w_{,x} + \theta_x\}. \end{aligned} \tag{2}$$

In this study, the displacement field is expressed in terms of the nodal variables in a four-node isoparametric shell element [17, 18].

$$\{U\} = \left\{U^0\right\} + \left\{U^1\right\}, \tag{3}$$

where $\{U^0\}$ and $\{U^1\}$ can be written as follows:

$$\begin{aligned} \left\{U^0\right\} &= \left\{u^0\, v^0\, w^0\, \theta_x^0\, \theta_y^0\right\}^T = \sum_{i=1}^{4} N_i^0 \left\{u_i\, v_i\, w_i\, \theta_{xi}\, \theta_{yi}\right\}^T, \\ \left\{U^1\right\} &= \left\{u^1\, v^1\, 0\, 0\, 0\right\}^T = \sum_{i=1}^{4} \left\{N_{ui}\, N_{vi}\, 0\, 0\, 0\right\}^T \theta_{zi}. \end{aligned} \tag{4}$$

Then, equation (3) can be expressed as as follows:

$$\{U\} = [N]\{d\}^e,\ [N] = \begin{bmatrix} N_1 & N_2 & N_3 & N_4 \end{bmatrix}, \tag{5}$$

where

$$[N_i] = \begin{bmatrix} N_i^0 & 0 & 0 & 0 & 0 & N_{ui} \\ 0 & N_i^0 & 0 & 0 & 0 & N_w \\ 0 & 0 & N_i^0 & 0 & 0 & 0 \\ 0 & 0 & 0 & N_i^0 & 0 & 0 \\ 0 & 0 & 0 & 0 & N_i^0 & 0 \end{bmatrix}, \quad (i = 1, 2, 3, 4). \tag{6}$$

The stiffness matrix of the plate structure can be written as follows [17, 18]:

$$\left[K_p\right]^e = \int \left[B_p\right]^T [D] \left[B_p\right] dA, \tag{7}$$

where $[B_p]$ is

$$\left[B_p\right] = \left[B_1 \quad B_2 \quad B_3 \quad B_4\right],$$

$$[B_i] = \begin{bmatrix} N_{i,x}^0 & 0 & 0 & 0 & 0 & N_{ui,x} \\ 0 & N_{i,y}^0 & 0 & 0 & 0 & N_{vi,y} \\ N_{i,y}^0 & N_{i,x}^0 & 0 & 0 & 0 & N_{ui,y} + N_{vi,x} \\ 0 & 0 & 0 & N_{i,x}^0 & 0 & 0 \\ 0 & 0 & 0 & 0 & N_{i,y}^0 & 0 \\ 0 & 0 & 0 & N_{i,y}^0 & N_{i,x}^0 & 0 \\ 0 & 0 & N_{i,x}^0 & N_{i,x}^0 & 0 & 0 \\ 0 & 0 & N_{i,y}^0 & 0 & N_{i,y}^0 & 0 \end{bmatrix}, (i = 1, 2, 3, 4). \tag{8}$$

2.2. Modelling of the Beam Element. The Timoshenko beam element is a two-node beam element that was developed using the Timoshenko beam theory and taking into account transverse shear deformation. Each node contains three displacement degrees u, v, and w and three rotation angles θ_x, θ_y, and θ_z. It is an element of the displacement degree of freedom w and the angle degree of freedom θ independently interpolated. It belongs to the C_0 type element, which is represented by the following interpolation:

$$w = \sum_{i=1}^{4} N_i w_i, \theta = \sum_{i=1}^{4} N_i \theta_i, \tag{9}$$

where w is the displacement of the ith node, θ is the angle of the ith node, n is the number of nodes, and N is the Lagrange interpolation function.

Similar to the shell element, the beam element can be expressed as follows:

$$k^e = k_s^e + k_b^e, \tag{10}$$

where k_s^e represents the element's overall stiffness, k_s^e represents its shear stiffness, and k_b^e represents its bending stiffness.

2.3. Elastic Boundary Stiffness and Internal Constraint Stiffness. The elastic coupling model of the coupled stiffened plate-cylindrical shell system is considered, as shown in Figure 2. The boundary around the stiffened plate is elastically connected with the closed cylindrical shell; that is, a pair of boundaries is elastically connected with the circular end plate and another pair of boundaries is elastically connected with the cylindrical shell. These pairs are expressed by four kinds of independent spring constraints (k_{cx}, k_{cy}, k_{cz}, and k_{sx}), while the elastic constraints on the boundary of the cylindrical shell are expressed by k_{sx}, $k_{s\theta}$, k_{sw}, and k_{sr}. The cylindrical shell is modelled using the cylindrical coordinate system, while the stiffening plate is simulated using the Cartesian coordinate system. Furthermore, u, v, and w represent the axial, tangential, and radial displacements, respectively. R, t_s, and L_s are the cylindrical shell's radius, thickness, and length, respectively. The elastic boundary of the cylindrical shell is described by the translation stiffness and rotational stiffness, and its strain energy is obtained as follows [19]:

$$U = \frac{1}{2}\int_0^{2\pi} \left[k_{sx0}u^2 + k_{s\theta 0}v^2 + k_{sw0}w^2 + k_{sr0}\left(\frac{\partial w}{\partial x}\right)^2 \right]_{x=0} Rd\theta + \frac{1}{2}\int_0^{2\pi} \left[k_{sxL}u^2 + k_{s\theta L}v^2 + k_{swL}w^2 + k_{srL}\left(\frac{\partial w}{\partial x}\right)^2 \right]_{x=L_s} Rd\theta. \tag{11}$$

The above equation can be further written as follows:

$$U = \frac{1}{2}\{\delta\}_e^T \{K_b\}_e \{\delta\}_e, \tag{12}$$

where $\{K_b\}_e$ can be written in detail as follows:

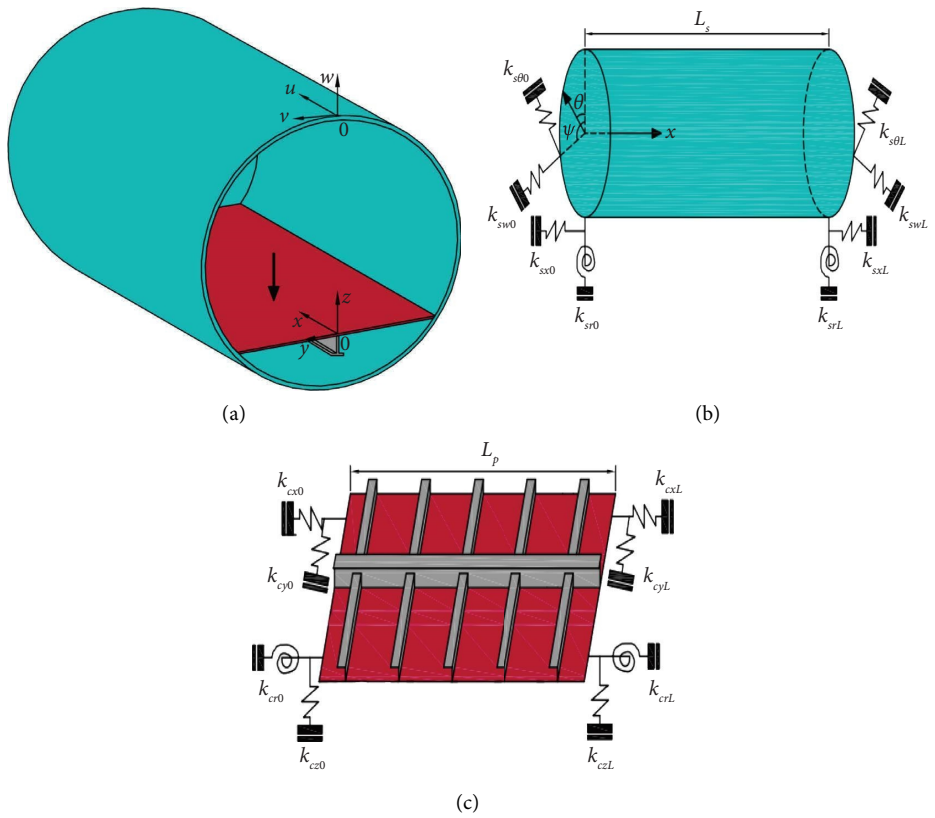

Figure 2: The elastic coupled plate-cylindrical shell system.

$$\{K_b\}_e = \int \left(\begin{array}{l} \frac{1}{2}k_{sx0}[N_u]^T[N_u] + \frac{1}{2}k_{s\theta 0}[N_v]^T[N_v] + \frac{1}{2}k_{sw0}[N_w]^T[N_w] + \frac{1}{2}k_{sr0}[N_w]^T\frac{\partial[N_w]}{\partial x} \\ \\ + \frac{1}{2}k_{sxL}[N_u]^T[N_u] + \frac{1}{2}k_{s\theta L}[N_v]^T[N_v] + \frac{1}{2}k_{swL}[N_w]^T[N_w] + \frac{1}{2}k_{srL}[N_w]^T\frac{\partial[N_w]}{\partial x} \end{array} \right) d\Gamma, \tag{13}$$

where $[N_u]$, $[N_v]$, and $[N_w]$ are form functions.

The total stiffness matrix of the elastic boundary can be expressed as follows:

$$[K_{sb}]_{x=0} = \begin{bmatrix} k_{sx0} & & & \\ & k_{s\theta 0} & & \\ & & k_{sw0} & \\ & & & k_{sr0} \end{bmatrix},$$
$$[K_{sb}]_{x=L} = \begin{bmatrix} k_{sxL} & & & \\ & k_{s\theta L} & & \\ & & k_{swL} & \\ & & & k_{srL} \end{bmatrix}. \tag{14}$$

Similarly, the internal constraint connection stiffness matrix of the coupled system $[K_{pb}]$ can be easily obtained, and the elastic boundary stiffness matrix and the coupling structure connection stiffness matrix are superimposed in the same coordinate system.

2.4. Modal Analysis. Ignoring the influence of the damping junction, the motion equation for the coupled system's modal analysis is expressed as follows:

$$[M]\{\ddot{U}\} + [K]\{U\} = 0. \tag{15}$$

Assuming harmonic vibrations, $\{U\} = \{U\}e^{i\omega_n t}$ and then

$$\left([K] - \omega_n^2[M]\right)\{U\} = 0, \tag{16}$$

where $[M]$ is the global mass matrix and $[K]$ is the global stiffness matrix.

This is a standard eigenvalue problem that is solvable for eigenvalues and eigenvectors.

$$[A]\{U\} = \lambda\{U\}, \tag{17}$$

where $[A] = [K]^{-1}[M]$ and $\lambda = (1/\omega_n^2)$.

2.5. Acoustic Radiation Model [18, 20]. The equation of motion of an elastic structure under a time-harmonic load can be written as follows:

$$\left(-\omega^2[M] + i\omega[C] + K\right)\{U\} = \{F\} - [G][A]\{P\}, \tag{18}$$

where $[A] = \int_S [N]^T[N]dS$, $[C]$ is damping matrices, and the vector $\{P\}$ can be written as follows:

$$\{P\} = [Z]\{v_n\}, \tag{19}$$

where $\{v_n\}$ is the normal velocity vector of the elastic structure and $[Z]$ is the acoustic impedance matrix.

$$\{v_n\} = [G]^T\{v\} = i\omega[G]^T\{U\}. \tag{20}$$

Therefore, the displacement vector of the elastic structure is

$$\{U\} = \left\{-\omega^2[M] + i\omega[C] + [G][A][Z][G]^T + [K_s]\right\}^{-1}\{F\}. \tag{21}$$

After solving the normal velocity $\{v_n\}$, the acoustic radiation power of the elastic structure can be calculated as follows:

$$W = \frac{1}{2}\int \mathrm{Re}\left(pv_n^*\right)ds. \tag{22}$$

In the above equation, an asterisk represents a complex conjugate.

3. Numerical Simulation Results

Generally, the vibration frequency of an elastic structure mainly depends on the material properties and the geometric size. Regarding the coupled system, it is also related to the relative position and connection form of each structure. In this section, a closed cylindrical shell containing a stiffened plate is taken as an example (for clear display, the seal plate is not drawn). As shown in Figure 1, ψ is the starting position of the stiffened plate, and L_p is the length of the stiffened plate. Its dimensions in the width direction are related to the coupling position. The thickness of the coupled system remain the same, that is, $t_p = t_s = t_e$, (the subscript s represents the cylindrical shell, p represents the stiffened plate, and e represents the end plate). The material of the structure is the same, and the stiffened plate structure is the same as the stiffened plate structure on the upper section. The T profile is arranged along the length direction of the cylindrical shell, and the L profile is arranged along the width direction of the stiffened plate. The fluid medium is air. The reference value of the velocity level is $1\,\mathrm{m}^2/\mathrm{s}^2$, and the reference value of the sound power level is 10^{-12} w.

The accuracy of the computation model must be confirmed. First, taking the natural frequencies of the cylindrical shell under rigid fixed boundary conditions as an example, all the stiffness coefficients at the edges of the cylinder are infinite. In this example, the value is 10^{15}. The dimension proportion relation of the cylindrical shell is $t_s/R = 0.002$, $L_s/R = 20$, and the natural frequencies parameter is $\Omega = \omega R\sqrt{\rho(1-\nu^2)/E}$. The calculation results are compared to those found in the published literature (Table 1). The numerical results are basically consistent with those in the literature.

Next, under elastic boundary conditions, this model is used to validate the natural frequency of cylindrical shell structures. One side is rigid and fixed, and the other side is elastically supported. Only the radial stiffness coefficient k_r changes, and the other elastic stiffness coefficients are set to zero, where $k = k_r/K$ and K is the internal rigidity of a cylindrical shell. The cylindrical shell dimensions are $L_s = 1.25\,\mathrm{m}$, $R = 0.25\,\mathrm{m}$, $t_s = 0.008\,\mathrm{m}$, $\rho = 7800\,\mathrm{kg/m}^3$, $E = 2.1\mathrm{e}11\,\mathrm{N/m}^2$, and $\nu = 0.3$. Table 2 displays a comparison between the computation findings and the literature. The numerical outcomes are essentially in line with those reported in the literature.

Finally, the vibration frequency of the elastic coupled plate-cylindrical shell system is compared to verify the accuracy of the internal connection stiffness. As an illustration, the elastic coupled plate-cylindrical shell structure is considered with simply supported constraints. Moreover, the coefficients of the elastic coupling stiffness between a flat plate and a cylinder are $k_{cx} = k_{cy} = k_{cz} = k_{cr} = 10^6$. The coupling position is $\psi = 115^o$, with $L_s = L_p = 1.27$ m, $t_s = t_p = 0.00508\,\mathrm{m}$, $\rho = 7500\,\mathrm{kg/m}^3$, $E = 2.1e11\,\mathrm{N/m}^2$, and $\nu = 0.3$. Table 3 presents the first 10 natural frequencies, and it is evident that the numerical outcomes mostly agree with those reported in the literature.

The stiffened plate and the cylindrical shell in the coupling structure have the following measurements: $L_s = L_p = 1\,\mathrm{m}$, $t_p = t_s = t_e = 0.002\,\mathrm{m}$, and $R = 0.18\,\mathrm{m}$. The structural material is steel, with properties of $\rho = 7800\,\mathrm{kg/m}^3$, $E = 2.06e11\,\mathrm{N/m}^2$, $\nu = 0.3$, and $\psi = 110^o$. The T-profile size is $2 \times 15/2 \times 6$ (unit: mm), the L-profile size is $10 \times 5 \times 2$ (unit: mm), the boundary stiffness coefficients of the cylindrical shell are $k_{sx} = k_{s\theta} = k_{sw} = k_{sr} = 10^{11}$, and the connection stiffness coefficients of the coupled structures are $k_{cx} = k_{cy} = k_{cz} = k_{cr} = 10^{11}$. Figures 3(a)–3(f) depict the first six modes of the elastically coupled plate-cylindrical shell system (part of the structure is hidden for the convenience of observation, as shown below).

According to the amplitude ratio of each part of the coupling structure, the modes in the figure can be roughly divided into two types. One mode is the stiffness control of a single structure. In Figures 3(a), 3(b), and 3(e), the modal amplitude of the stiffened plate is much larger than those of the cylindrical shell and the circular plate at both ends. In this instance, the modal amplitude of the stiffened plate-cylindrical shell coupling structure is controlled by the stiffened plate structure because the stiffened plate has a larger side length. Compared to the cylinder and circular plate, its bending stiffness is lower. The stiffened plate in this scenario receives boundary stiffness from the circular plate and the cylindrical shells at each end, and the circular plate and the cylindrical shell at both ends possess enough rigidity to control the stiffened plate's border movement.

In Figures 3(c) and 3(d), the modal amplitudes of the circular plates at both ends are much larger than those of the cylindrical shell and the stiffened plates. The modes of the coupling structure are controlled by the circular plates at both ends. The others are the coupled modes of multiple structural stiffness controls. Figure 3(f) shows the coupled modes of the structure. The amplitudes of each structural

Table 1: Natural frequencies of a cylinder with clamp boundary conditions.

m	n	Flügge theory [21]	Zhang et al. [22]	Zhang et al. [23]	Present solution
1	1	0.0344	0.03487	0.03488	0.03295
	2	0.01204	0.01176	0.01173	0.01167
	3	0.00722	0.00708	0.00711	0.00710
	4	0.00905	0.00902	0.00895	0.00905
	5	0.01377	0.01377	0.01412	0.01385
2	1	0.08484	0.08724	0.08485	0.07966
	2	0.03162	0.03155	0.03176	0.03066
	3	0.01603	0.01586	0.01585	0.01572
	4	0.01233	0.01224	0.01232	0.01224
	5	0.01484	0.01482	0.01486	0.01489

Table 2: Natural frequencies for a cylindrical shell with the clamped-elastic condition.

Modal orders		$\hat{k} = 0$	$\hat{k} = 0.01$	$\hat{k} = 0.1$	$\hat{k} = 1$	$\hat{k} = 1e6$	$\hat{k} = 1e8$
1	Dai [24]	131.99	183.01	298.01	315.07	315.15	315.15
	Present solution	131.49	182.88	298.45	314.88	315.48	315.48
2	Dai [24]	249.82	278.17	310.07	339.86	343.43	343.43
	Present solution	248.97	277.68	309.55	340.31	345.52	345.52
3	Dai [24]	262.81	279.76	364.98	473.26	491.36	491.36
	Present solution	262.82	279.79	365.56	476.62	490.28	490.28
4	Dai [24]	377.00	404.12	490.35	491.64	501.06	501.08
	Present solution	375.67	403.13	488.90	490.14	506.01	506.01

Table 3: Natural frequencies of a plate-cylindrical shell system with a clamped-elastic support.

Modal orders	Dai [19]	Present solution	Error (%)
1	49.906	49.557	0.699
2	59.483	59.251	0.390
3	60.990	60.990	0.000
4	86.696	86.576	0.138
5	99.008	98.535	0.478
6	116.00	115.48	0.448
7	134.25	134.16	0.067
8	147.72	147.15	0.386
9	196.29	195.62	0.341
10	200.20	200.09	0.055

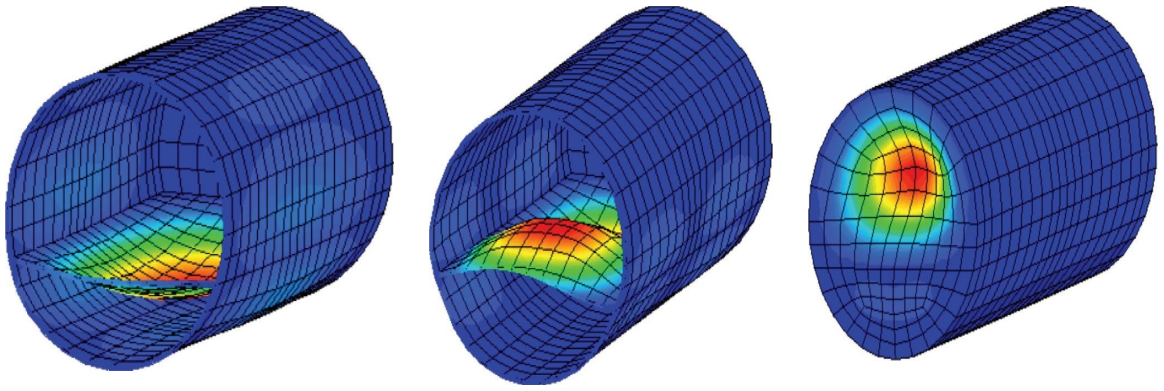

(a) (b) (c)

Figure 3: Continued.

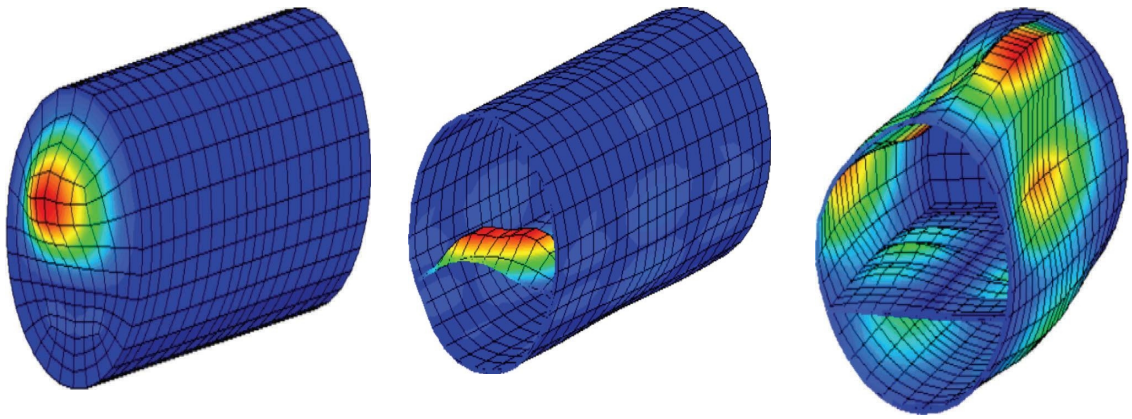

(d) (e) (f)

Figure 3: (a–f) The first six modes of the elastic coupled plate-cylindrical shell system.

mode in the coupled structure are equivalent or nonnegligible.

The influence of the internal connection stiffness of the elastic coupled stiffened plate-cylindrical shell system on these two modes is further explained below. Only the elastic connection stiffness is changed. It is assumed that the stiffness coefficients in all directions increase in proportion from the free end to the rigid fixed end. Taking the antisymmetric coupling mode as an example, this mode is mainly the elastic coupling deformation between the stiffened plate and the cylindrical shell, and the circular plate just slightly deforms at each end.

The variation curve of modal frequencies as a function of the stiffness coefficient is shown in Figure 4. The figure demonstrates that when the rigidity coefficient k is from 0 to 10^2, the modal frequencies of this coupled structure change a little because the stiffness coefficients in all directions are small at this time, the cylindrical shell and the stiffened plate cannot be effectively connected, and the modes of the coupled structure are mainly controlled by the cylindrical shell. Stiffened plates have insignificant modal amplitudes, as shown in Figure 5(a).

When the stiffness coefficient connection k ranges from 10^2 to 10^{10}, the vibration frequencies increase rapidly with increasing stiffness coefficients (Figure 4), the stiffened plate has a greater rise in its modal amplitude, and the stiffened plate and the cylindrical shell exhibit coupled vibration as a whole, as shown in Figures 5(b) and 5(c). At this stage, the coupling modes of the structure are sensitive to the stiffness coefficient. At this stage, the influence of the constraint structure dynamic performance has practical significance to the actual structure. For example, the actual structural connection constraints are often complicated. Moreover, the connection stiffness between the ship deck and the side shell plate is neither freely supported nor rigidly fixed but between a free support and rigid fixation, and the constraint between them, which is often called an elastic constraint, can be considered as $k = 10^8$ (Figure 1).

When the stiffness coefficient connection k ranges from 10^{10} to 10^{15}, the coupling modal frequencies of the structure are basically unchanged at this stage with the increase in the

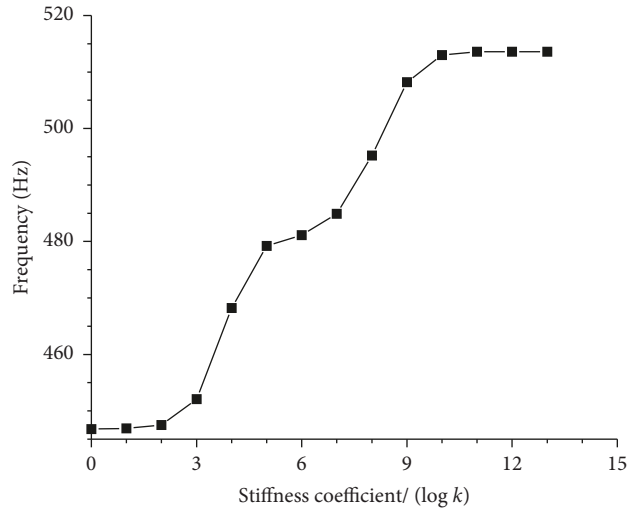

Figure 4: Antisymmetric modal frequency curve of the elastic coupled stiffened plate-cylindrical shell system with different stiffness coefficients.

stiffness coefficient (Figure 4). Because the stiffness coefficient is sufficiently large at this time, the connection among the stiffened plate, the circular plate, and the cylindrical shell at both ends is equivalent to rigid fixation, and the connection between each structure no longer has relative translation or rotation, which is equivalent to the welding situation in the actual structure. As shown in Figure 5(d), an organic overall structure has been formed.

The other type of mode is the single structural mode; that is, with an increasing connection stiffness, the vibration mode of the coupled system is always a single structural mode. Taking the first mode as an example, as shown in Figure 6, the vibration mode of the coupled structure resembles that of the stiffened plate with the increase in the connection stiffness in each direction. When the connection stiffness between the coupling structures is large, the vibration frequency of the structure is 159 Hz, which is significantly different from that of the stiffened plates when the boundary stiffness around the stiffened plates is fixed

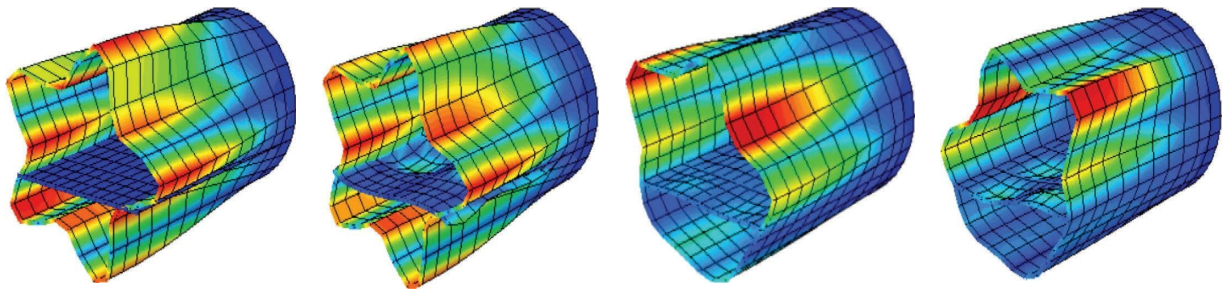

Figure 5: Coupled modes of the elastic coupled stiffened plate-cylindrical shell system with different stiffness coefficients. (a) $k = 10^1$. (b) $k = 10^4$. (c) $k = 10^8$. (d) $k = 10^{15}$.

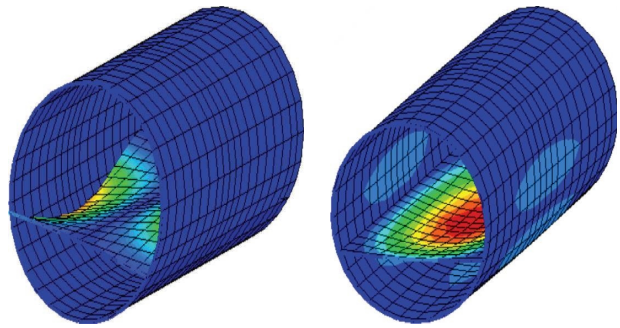

Figure 6: Single structure mode of the elastic coupled stiffened plate-cylindrical shell system with different stiffness coefficients. (a) $k = 10^1$. (b) $k = 10^{15}$.

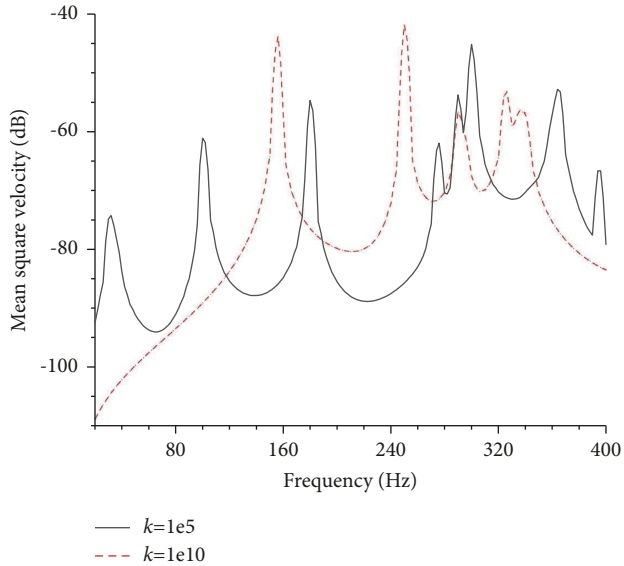

Figure 7: Mean square velocity of an elastic coupled structural system with different stiffness coefficients.

(289 Hz). The reason is that the cylindrical shell and the round plates at both ends of the structure are not sufficiently "rigidly fixed" around the stiffened plates, and the boundary around the stiffened plates can still translate and rotate in a limited range.

Then, it is assumed that the point excitation force acts on the midpoint of the internal plate at the cylindrical shell, and when the elastic connection stiffness of the coupling structure is between 10^5 and 10^{10}. Figures 7 and 8 depict the mean square velocity (MSV) and radiated sound power

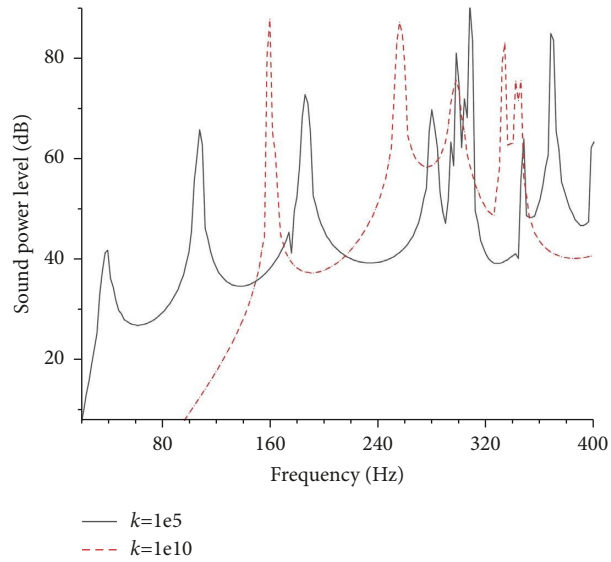

Figure 8: Sound power level of an elastic coupled structural system with different stiffness coefficients.

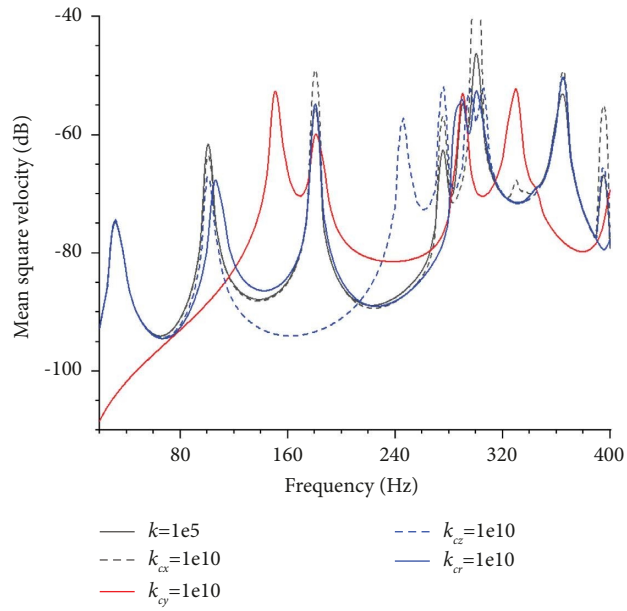

Figure 9: Mean square velocity of an elastic coupled structural system with a single stiffness coefficient change.

(RSP) curves, respectively. The results show that the coupling stiffness has a substantial impact on the acoustic and vibrational forces of the coupled structure.

First, when the connection stiffness coefficient increases, the number of resonant frequencies of the connected structure reduces as the connection stiffness increases, and the self-vibration modes of each structure gradually become the coupled vibration modes of the structure. Second, when the connection stiffness increases, the peaks of the curves obviously increase. This is because the impedance matching between the structures is improved with an increasing connection stiffness, which is conducive to vibration energy propagation. Third, the curves of the structure both move towards high frequencies. This is because the increase in the stiffness of the connection leads to an increase in the frequency of the structure.

To explore the impact of the coupling spring stiffness on the acoustic and vibration performance of a coupled structure separately, the stiffness value of one coupling spring was modified in turn, while the stiffness of the other coupling spring was set to 1*e*5. The MSV curve and the RSP curve of the elastic coupled structural system are shown in Figures 9 and 10. While the coupling stiffness in the direction of k_{cy} has a significant impact on the vibration and sound radiation of the coupled structure, the coupling stiffnesses in the other directions have a much less impact on the structural system's ability to dampen vibration and sound. That is, the supporting coupling stiffness between the

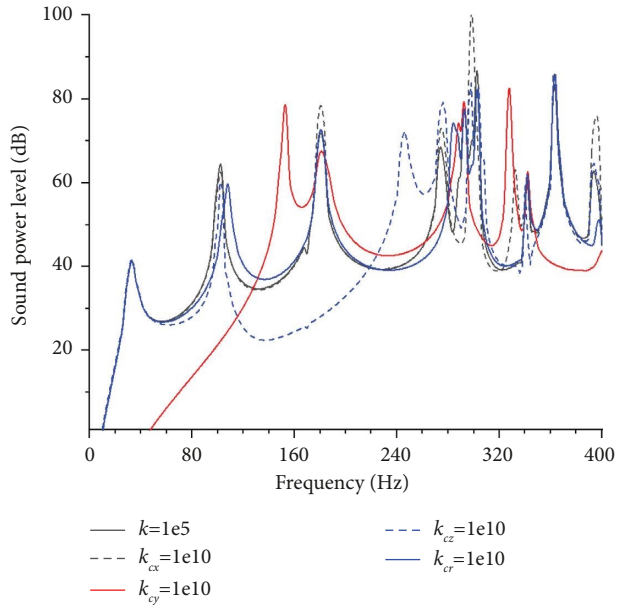

Figure 10: Sound power level of an elastic coupled structural system with a single stiffness coefficient change.

elastic plate and the cylindrical shell structure plays a major role in the vibration energy transfer. In fact, the bending vibration transfer of the inner plate is what truly constitutes the vibration coupling transfer in the y direction of the structure. Therefore, in the actual structure, it is recommended that the support's strength and stiffness be decreased to lessen the vibration sound radiation produced by the structure. One way to do this would be to install rubber gaskets.

4. Summary

In this research, we build a calculation model of a coupled plate-cylindrical shell system to investigate the effect of internal constraint stiffness on this performance. The following conclusions are the most important:

(1) According to the amplitude ratio of each part of the coupled structures, the modes can be roughly divided into two types. One mode is single-structure stiffness control, and the other type is the coupled mode of multiple-structure stiffness control.

(2) The coupled modes are closely related to the connection stiffness, while the single structural modes are basically independent of the connection stiffness.

(3) When the connection stiffness increases, the MSP curve and the RSP curve of the coupled structure approach a high frequency and the resonance peak value increases, while the number of resonant frequencies decreases.

(4) The supporting coupling stiffness between the elastic coupled structures plays an important role in the vibration energy transfer.

Data Availability

The data used to support the findings of this study are included within the article.

Conflicts of Interest

The authors declare that there are no conflicts of interest.

Acknowledgments

This study was sponsored by the Natural Science Foundation of Chongqing, China (Grant No. CSTB2022NSCQ-BHX0046).

References

[1] S. Javed, F. Mukahal, and M. A. Salama, "Free vibration analysis of composite conical shells with variable thickness," *Shock and Vibration*, vol. 2020, Article ID 4028607, 2020.

[2] O. Civalek, S. Dastjerdi, and B. Akgoz, "Buckling and free vibrations of CNT-reinforced cross-ply laminated composite plates," *Mechanics Based Design of Structures and Machines*, vol. 50, no. 6, pp. 1914–1931, 2022.

[3] E. Sobhani, A. Arbabian, O. Civalek, and M. Avcar, "The free vibration analysis of hybrid porous nanocomposite joined hemispherical–cylindrical–conical shells," *Engineering with Computers*, vol. 38, no. S4, pp. 3125–3152, 2022.

[4] O. Civalek and M. Avcar, "Free vibration and buckling analyses of CNT reinforced laminated non-rectangular plates by discrete singular convolution method," *Engineering with Computers*, vol. 38, no. S1, pp. 489–521, 2022.

[5] X.-Q. Li, G.-C. Bai, L.-K. Song, and W. Zhang, "Nonlinear vibration analysis for stiffened cylindrical shells subjected to electromagnetic environment," *Shock and Vibration*, vol. 2021, Article ID 9983459, 26 pages, 2021.

[6] J. Missaoui and L. Cheng, "Vibroacoustic analysis of a finite cylindrical shell with internal floor partition," *Journal of Sound and Vibration*, vol. 226, no. 1, pp. 101–123, 1999.
[7] D. S. Li, L. Cheng, and C. M. Gosselin, "Analysis of structural acoustic coupling of a cylindrical shell with an internal floor partition," *Journal of Sound and Vibration*, vol. 250, no. 5, pp. 903–921, 2002.
[8] Z. H. Wang, J. T. Xing, and W. G. Price, "A study of power flow in a coupled plate-cylindrical shell system," *Journal of Sound and Vibration*, vol. 271, no. 3-5, pp. 863–882, 2004.
[9] Z. Zhao, M. Sheng, and Y. Yang, "Vibration transmission of a cylindrical shell with an interior rectangular plate with the receptance method," *Advances in Acoustics and Vibration*, vol. 2012, Article ID 581769, 9 pages, 2012.
[10] A. Clot, J. Romeu, R. Arcos, and S. R. Martín, "A power flow analysis of a double-deck circular tunnel embedded in a full-space," *Soil Dynamics and Earthquake Engineering*, vol. 57, no. 12, pp. 1–9, 2014.
[11] M. S. Zou, S. X. Liu, and L. B. Qi, "An analytical formulation for the underwater acoustic radiation of a cylindrical shell with an internal flexural floor based on the reciprocity theorem," *Applied Acoustics*, vol. 154, pp. 18–27, 2019.
[12] J. Deng, N. Gao, L. Tang, H. Hou, K. Chen, and L. Zheng, "Vibroacoustic mitigation for a cylindrical shell coupling with an acoustic black hole plate using Gaussian expansion component mode synthesis," *Composite Structures*, vol. 298, Article ID 116002, 2022.
[13] L. Tian, G. Jin, T. He et al., "A hybrid analytic-numerical formulation for the vibration analysis of a cylindrical shell coupled with an internal flexural floor structure," *Thin-Walled Structures*, vol. 183, Article ID 110382, 2023.
[14] T. Y. Zhao, K. Yan, H. W. Li, and X. Wang, "Study on theoretical modeling and vibration performance of an assembled cylindrical shell-plate structure with whirl motion," *Applied Mathematical Modelling*, vol. 110, pp. 618–632, 2022.
[15] Y. S. Lee and M. H. Choi, "Free vibrations of circular cylindrical shells with an interior plate using the receptance method," *Journal of Sound and Vibration*, vol. 248, no. 3, pp. 477–497, 2001.
[16] Y. X. Zhang and K. S. Kim, "Geometrically nonlinear analysis of laminated composite plates by two new displacement-based quadrilateral plate elements," *Composite Structures*, vol. 72, no. 3, pp. 301–310, 2006.
[17] J. F. Zhu and G. Zheng, "A new 4-node C quadrilateral plate/shell element with drilling degree of freedom," *Chinese Journal of Computational Mechanics*, vol. 17, no. 3, pp. 287–292, 2000.
[18] Y. G. Sun, "Vibration and acoustic radiation of stiffened plates subjected to in-plane forces," *Advances in Civil Engineering*, vol. 2022, Article ID 9917664, 10 pages, 2022.
[19] L. Dai, *Study on Dynamic Behavior and Acoustic Radiation for the Coupling Structure of Cylindrical Shells with Complex Boundary Conditions*, Harbin Engineering University, Harbin, China, 2013.
[20] S. Li, "Modal models for vibro-acoustic response analysis of fluid-loaded plates," *Journal of Vibration and Control*, vol. 17, no. 10, pp. 1540–1546, 2011.
[21] R. D. Blevins, *Formulas for Natural Frequency and Mode Shape*, Var Nostrand Reinhold Co, New York, NY, USA, 1979.
[22] X. M. Zhang, G. R. Liu, and K. Y. Lam, "Vibration analysis of thin cylindrical shells using wave propagation approach," *Journal of Sound and Vibration*, vol. 239, no. 3, pp. 397–403, 2001.
[23] W. Zhang, Z. Fang, X. D. Yang, and F. Liang, "A series solution for free vibration of moderately thick cylindrical shell with general boundary conditions," *Engineering Structures*, vol. 165, pp. 422–440, 2018.
[24] L. Dai, T. Yang, J. Du, W. Li, and M. Brennan, "An exact series solution for the vibration analysis of cylindrical shells with arbitrary boundary conditions," *Applied Acoustics*, vol. 74, no. 3, pp. 440–449, 2013.